# Using Implicit Solvent in *Ab Initio* Electrochemical Modeling: Investigating Li⁺/Li Electrochemistry at a Li/Solvent Interface

Nicolas Lespes[†,‡] and Jean-Sébastien Filhol[*,†,‡]

[†]Institut Charles Gerhardt—CNRS 5253 and Université de Montpellier, Place Eugène Bataillon, 34 095 Montpellier Cédex 5, France
[‡]Réseau sur le Stockage Electrochimique de l'Energie (RS2E), CNRS FR3459, 80039 Amiens Cedex, France

ABSTRACT: This paper focuses on the use of implicit solvent in electrochemical density functional theory (DFT) calculations. We investigate both the necessity and limits of an implicit solvent polarizable continuum model (PCM). In order to recover the proper electrochemical behavior of the surface and, in particular, a proper potential scale, the solvent model is determined to be mandatory: in the limit of a high dielectric constant, the surface capacitance becomes independent of the interslab space used in the model and, therefore, the electrochemical properties become intrinsic of the interface structure. We show that the computed surface capacitance is not only dependent on the implicit solvent dielectric constant, but also on the solvent cavity parameter that should be precisely tuned. This model is then applied to the Li/electrolyte interface in order to check its ability to compute thermodynamic equilibrium properties. The use of a purely implicit solvent approach allows the recovery of a more reasonable equilibrium potential for the Li⁺/Li redox pair, compared to vacuum approaches, but a potential that it is still off by 1.5 V. Then, the inclusion of explicit solvent molecules improves the description of the solvent−Li⁺ chemical bond in the first solvation shell and allows recovery of the experimental value within 100 mV. Finally, we show that the redox active center involves the first solvation shell of Li⁺, suggesting a particular pathway for the observed solvent dissociation in Li-ion batteries.
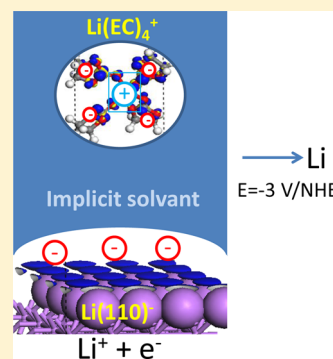
I. INTRODUCTION

The electrochemical interface is fundamental to understanding electrochemical reactions either for electrocatalysis applications, corrosion, and electroplating or for energy conversion or storage devices such as fuel cells or Li-ion batteries.[1,2] Nevertheless, this interface is extremely complex to model, not only because of the occurring electrochemical effects, but also because of the complexity of the electrode−solvent interactions. Classical models such as Stern/Gouy−Chapmann/Helmoltz reproduce the electric behavior fairly well by introducing more or less complex descriptions of the double layer (Helmholtz plane, diffuse layer, etc.);[3] nevertheless, they fail to include the chemical dimension of bond modification occurring at the interface with the potential change. In contrast, *ab initio* approaches describe the chemical bonding and reactivity at the interface with good accuracy[4−6] but, most of the time, are oblivious to the electric/electrochemical dimension. We have previously developed an approach using an homogeneous compensating background charge,[7−9] which allows one to include electrochemical effects at the *ab initio* density functional theory (DFT) level, as have other groups.[8,10−14] This method allows the recovery of all of the fundamental properties of the surface free electrochemical energy $F = E − qV$ (where E is the surface energy, q the charge, and V surface potential) and allows one to study electrochemical phenomena easily in a vacuum environment. The bias was induced by charging the surface and compensating this charge by a homogeneous charge distribution[8,10−13] to keep the unit cell neutral and to induce the local electrochemical effects.

This very simple approach has been successful into gaining quantitative insight into many electrochemical phenomena occurring mainly under vacuum conditions (Stark effect,[8,14] water organization[15−17]), while it gives very similar results to more complex methods.[13,14] However, all of the vacuum electrochemical approaches have an important drawback: the surface capacitance is dependent on the vacuum size (or equivalent) used in the calculation (i.e., the position of the reference potential relatively to the surface) and, therefore, is NOT an intrinsic parameter of the interface as it is found in the case of most of the experimental electrochemical setups in the high electrolyte concentration limit. The vacuum size then must be adjusted in order to be in the proper capacitance range for the studied phenomena. One way to recover a capacitance that is only dependent on the surface, but not on the unit cell limits, and give a reliable potential scale, was to add many layers of (strongly polar) solvent, as done previously.[7] However, this approach is computationally demanding and does not allow a description of the solvent in its full structural and time-dependent complexity.[18,19] A less-expensive way is to use an implicit continuum representation of the solvent molecules, as routinely done in molecular calculations,[20,21] but also in some condensed matter approach.[22,23] Nevertheless, if the limits of the implicit solvent models are well-controlled for molecular approaches and neutral surfaces, it is not the case for a condensed matter electrochemical interfacial system.

In the present paper, we couple an electrochemical approach with a newly implemented polarizable continuum model (PCM)[24] as an implicit solvent model.[25] We first focus on the impact of the parameters controlling the implicit PCM solvent on the electrochemical results. We particularly focus on the interface between the Li(110) surface and ethylene carbonate (EC) solvent that not only corresponds to the reference electrode for Li/ion battery materials, but also is of technological importance. First, Li/carbonate-solvent interfaces are electrochemically unstable upon reduction, because of dendritic growth,[26−28] resulting in catastrophic battery failure: this prevents the use of metal Li in most Li-ion batteries, where it is often replaced by a graphite-intercalated compounds, leading to an order-of-magnitude loss of stored energy density.[29] Carbonate solvents then also have a tendency to decompose[30−33] upon reduction, participating in the formation of a solid electrolyte interface (SEI).[34]

We study how the two main parameters controlling the PCM (namely, the dielectric constant and the cavity parameter) impact the interface capacitance. We show that, for high dielectric constant, the surface properties become independent of the interslab space size used in the model unit cell as expected in the limit of a high electrolyte concentration. We then apply this approach to model the equilibrium potential of a Li$^+$/Li interface and to investigate the impact of implicit/explicit solvent on the equilibrium electrochemical potential and on the redox active center.

II. COMPUTATIONAL DETAILS

The periodic electronic structure calculations were performed using density functional theory (DFT) within the PBE[35] generalized gradient approximation and projected augmented wave (PAW[36,37]) pseudo-potentials, as implemented in the VASP code.[37−39] (4 × 4) Li(110) symmetric slabs containing 7 Li layers were built.[40,41] This surface orientation was previously found to be the most stable.[41] Periodic surfaces were separated by a vacuum of at least 19.4 Å that was double for some calculations (*vide infra*). During structural relaxations, the middle Li layer was kept frozen to bulk parameter while all other atoms were allowed to relax. After relaxation bulk parameters were recovered at the middle of the Li slab. Compounds were added symmetrically on both sides in order to avoid long-range electrostatic interactions between periodic images arising from periodic boundary conditions and to deal with only one type of surface energetic. (3 × 3 × 1) Γ-centered k-points meshes were used. The energy cutoff was set to 450 eV. For all optimized structures, the residual forces on atoms after structural relaxation were lower than 0.01 eV Å^{-1}. All energies are referenced to the bare uncharged Li(110) surface and to EC molecule solvated in the implicit solvent. The electrochemical calculations have used the approach described in ref 8. The middle of the interslab space layer (z_{ref}) potential is used as the reference potential because (a) there is no electron density and (b) at this position, the electrostatic potential V is a local extremum ($\partial V/\partial z(z_{ref}) = 0$), regardless of the charging. The chosen reference for all given potentials is the vacuum potential. A shift from vacuum scale toward normal hydrogen electrode (NHE) can be estimated using the expression $V_{NHE} = V_{vacuum} − V_{vac.ref}$, where $V_{vac.ref} = 4.6$ V.[42,43] The implicit solvent model, used in the present paper, was implemented in the VASP code by another group.[25,44] It describes the solvent by an effective dielectric continuous response outside of the atomic cavities defined by an electronic

density cutoff parameter (n_c). In this model, an extra effective surface tension (τ) can be added to include effectively nonelectrostatic contributions, but since the cavity shape does not change much in the studied surface, we have neglected its effects for comparison between similar surfaces, to focus on the other PCM parameters.

For the initial part of this study, a value of $n_c = 2.5 \times 10^{-4}$ Å^{-3} was used with different ϵ_r, whereas, for the following parts, $\epsilon_r = 89.9$ (experimental dielectric constant of the ethylene carbonate) was chosen and the influence of n_c investigated.

Throughout the paper, the differential capacitance is given by $C = −1/S(\partial^2 F/\partial V^2)$, where F is the free electrochemical energy of the slab, V the surface Galvani potential, and S the total surface area. The potential of zero charge is always the maximum of the parabola-shape representative curves of the free electrochemical energies (a zero (0) was added in most of the figures to emphasize this particular potential). The typical charge step is 8×10^{-4} e Å^{-2}.

III. EFFECT OF THE PCM AND ELECTROCHEMICAL PARAMETERS

Classically, the main parameter of the PCM model is the dielectric constant ϵ_r, but the value found for neutral systems is not directly transferrable to charged ones.

(A). Effect on the Dielectric Constant. The free electrochemical energy was computed for a Li/implicit-solvent interface for different ϵ_r. The results are given in Figure 1a. In

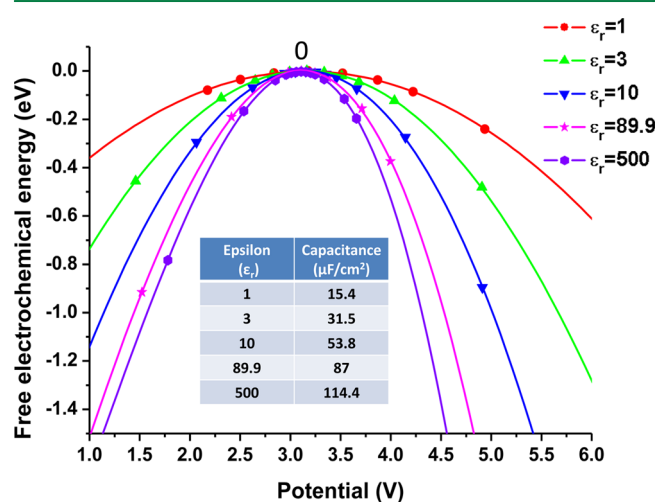| Epsilon (ϵ_r)	Capacitance (µF/cm^2)
1	15.4
3	31.5
10	53.8
89.9	87
500	114.4

Figure 1. Evolution of the free electrochemical energy at a Li/implicit solvent interface as a function of the potential (referred to vacuum potential) and as a function of the solvent dielectric constant. Inset: zero-charge capacitance as a function of the solvent dielectric constant.

all cases, the free energy has the standard inverted parabola-shape centered at the potential of zero charge, as expected from thermodynamic relationships. With changes in the ϵ_r value, from 1 to 500, the zero-charge potential shifts toward lower values with a maximal decrease of 70 mV associated with a weak surface energy stabilization of 3 meV. The change in the zero-charge potential (V_0) can be linked with a modification of the surface dipole (p_0)[8] as $p_0 \approx −\epsilon_0 S V_0$, where S is the surface area. The implicit solvent screens the surface electronic density, slightly decreasing the electronic density spilling into interslab space and, therefore, the surface dipole. The uncharged system energy is only weakly stabilized by the polarizable media as only a weak electronic tail is leaking into the PCM region.

The charged surface free electrochemical energies are strongly stabilized by the interactions with the implicit solvent with increasing ϵ_r. The reason is that the surface capacitance is increasing by 1 order of magnitude with an increase of 2 orders of magnitude in ϵ_r (see Figure 1b), tending toward a limit value of $\sim$120 μF cm^{-2}. While, for $\epsilon_r = 1$, the surface free electrochemical energy is almost strictly parabolic with V; increasing ϵ_r leads to third-order polynomial contributions associated with a more efficient stabilization of positive charges, compared to negative ones (*vide infra*).

The change of the surface capacitance can be investigated through the (x,y)-plane average electrostatic force potential, as a function of the surface distance (see Figure 2).
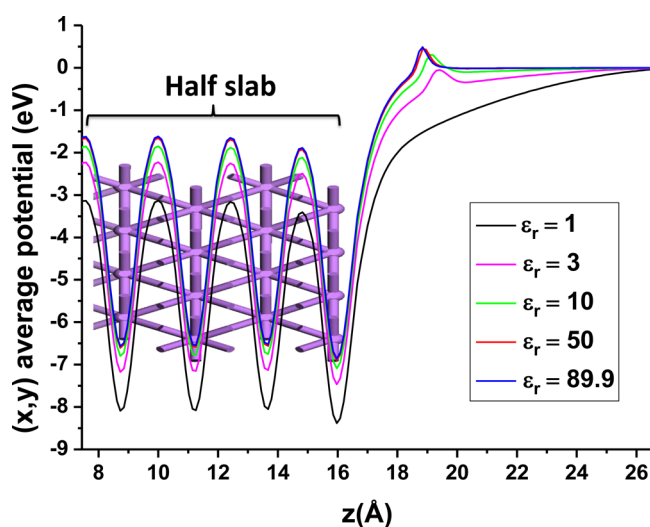

Figure 2. Evolution of the (x,y)-plane average of the electrostatic potential as a function of distance, and of the solvent dielectric constant at a surface charge of 0.004 e Å^{-2}. The reference potential is set at $z = 26.5$ Å. The structure of the slab is superposed on the potential curves.

The black line in Figure 2 gives the potential of the surface in the absence of implicit solvent for a positive surface charge of 0.004 e Å^{-2}. The metal part is below 17 Å and the interslab part is above 17 Å. With no PCM, the potential is increasing in the entire interslab space part. The other lines give the potential evolution for increasing ϵ_r from 3 to 89.9. In all of these curves, three domains are observed: the metal part below 17 Å; an intermediate part between 17 Å and $\sim$19 Å, and the implicit solvent region above 19 Å that is characterized by a "bump" in the potential. This "bump" in the potential is directly linked with the implicit solvent dipolar response to the surface charge: for a positively charge slab as presented therein, the PCM polarization leads to a negative charging at the cavity part pointing toward the surface associated with a positive tail toward the vacuum, leading to a local increase in the potential curve close the cavity limit. It is worth noticing that the bump delimiting the implicit solvent zone is shifting toward the surface with increasing ϵ_r from position at 19.4 Å ($\epsilon_r = 3$) to 18.5 Å for very large values ($\epsilon_r = 89.9$): a higher dielectric constant localizes the negative response (for positively charged surface) of the dielectric medium closer to the cavity limit.

With increasing ϵ_r, the potential in the metal part is homogeneously shifted upward, but tends toward a limit value for higher ϵ_r. In the solvent part, the potential is obtained by dividing by ϵ_r (the value without PCM), as expected from classical electrostatics. The maximum potential change relative to vacuum potential in this region then decreases from $\sim$2 V for $\epsilon_r = 1$ to $\sim$22 mV for $\epsilon_r = 89.9$ and tends to zero for higher ϵ_r. Finally, in the intermediate part at 18 Å, the local electric field value (derivative of the potential curve) remains constant at $\sim$0.79 V Å^{-1}, purely controlled by the surface charge density. For high ϵ_r, the decrease in potential, relative to the vacuum reference, is dominated by the intermediate region and tends toward a constant value ΔV ($\Delta V \approx \rho r_c$, where ρ is the surface charge and r_c is the cavity size). The surface capacitance behaves as $C \sim 1/r_c$ for large ϵ_r. For sufficiently high values of ϵ_r, and for a given cavity size r_c, as the potential change inside the implicit region drops to zero, the electrochemical potential becomes only dependent on the surface charge, leading to an almost-constant surface capacitance. However, in contrast to uncharged calculations, the cavity size parameter r_c, which is controlled by the parameter n_c, is expected to have a strong impact on the electrochemical calculations, as shown in the next subsection.

(B). Effect of the Parameter n_c. The cavity size n_c is a parameter that roughly controls the distance between the system to be solvated and the implicit solvent. The smaller this parameter is, the closer the dielectric region of the PCM comes to the solute. This can be seen in the evolution of the electrostatic potential in the unit cell as a function of n_c, as presented in Figure 3b. In our studied range ($n_c = 0.25 \times 10^{-4}$–$2.5 \times 10^{-4}$ Å^{-3}), the typical distance from the surface to the dielectric solvent changes from $\sim$3 Å to 2 Å. The effect of n_c on the zero-charge properties is weak: the zero-charge energy is mostly unchanged and the zero-charge potential shifts by 20 mV. However, the effect on charged systems is important as a smaller n_c leads to a more stable free electrochemical energy (see Figure 3a), associated with a strong increase of the surface differential capacitance (multiplied by a factor 2 in this range). As seen above, the capacitance is directly linked with the cavity size as $C \approx 1/r_c$ and, therefore, with n_c. The parameter n_c then is critical in electrochemical modeling and would need to be correctly adjusted to obtain the proper capacitance. We have used a parameter of 2.5×10^{-4} Å^{-3}, which corresponds to a typical distance between the negative carbonate part of an adsorbed EC molecule and the Li surface ($\sim$3.0 Å).

(C). Influence of the Interslab Space Size. The parameter that is directly setting the surface capacitance in vacuum calculations is the vacuum size: for these calculations, the surface capacitance varies as $1/d_{vac}$, where d_{vac} is the vacuum size in the unit cell. The electrochemical responses of two identical Li slabs, only differing by their interslab space size (one being the double of the other) were computed for vacuum and PCM and are shown in Figure 4. For these two systems, zero-charge potentials are equal and zero-charge energies only differ by 5 meV. For the systems under vacuum, the representative parabolas are very different, as larger d_{vac} values lead to less-stable charged surfaces. As expected, decreasing d_{vac} by a factor of $\sim$2 leads to a doubling of the surface capacitance. In the case of implicit solvent, the representative parabolas of the free electrochemical energies are extremely close and the capacitances only differ by 3%. When using an implicit PCM solvent (with high enough dielectric constant), capacitance becomes an intrinsic property of the surface that is almost independent of the interslab size in the modeling, whereas, in the case of a vacuum, this size is the determining parameter for capacitance.
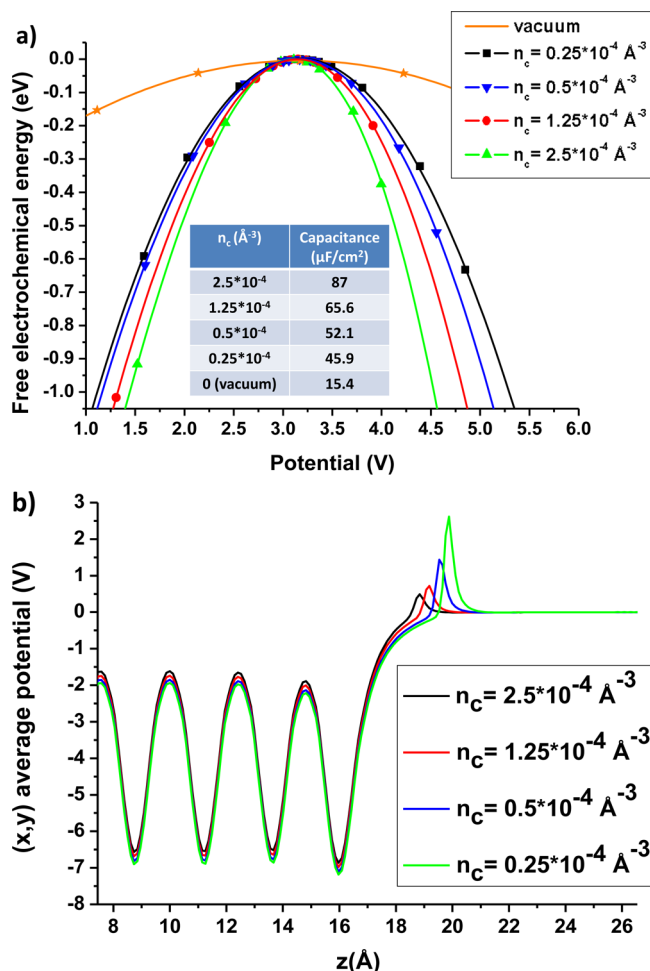
Figure 3. Effect of the cavity size parameter n_c on (a) the free electrochemical energy, as a function of the electrochemical potential (the inset gives the zero-charge capacitance for different n_c), and (b) on the (x,y)-plane average electric potential in the unit cell.
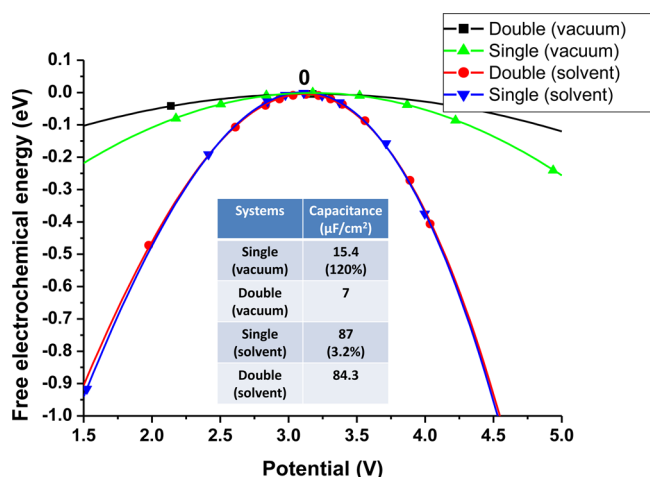

Figure 4. Evolution of the free electrochemical energy with potential for two interslab z-sizes (20 and 40 Å) under vacuum and in an implicit solvent. The evolution of the surface capacitance is given in the inset. Solvent parameters are $n_c = 2.5 \times 10^{-4}$ Å^{-3} and $\varepsilon_r = 89.9$.

(D). Differential Capacitance. The differential capacitance for a bare Li surface is given in Figure 5, in the case of an implicit solvent. While it is constant for a surface without PCM,
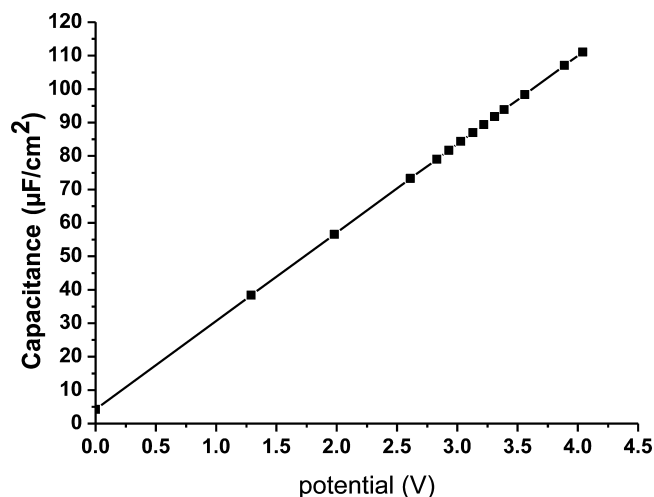

Figure 5. Evolution of the differential capacitance, as a function of the potential vs vacuum.

with PCM it has a strong linear dependency. Experimentally, a strong dependence of the differential capacitance with potential is well-known (modifications by a factor of 2−4[45] for a few hundred millivolts) and are associated[46] with changes in the double layer (solvation-specific adsorption, solvent reorientation, etc.). In the present case, the linear behavior is partly artifactual: at low potential, the electron spilling increases at the interface, leading to an increased electron density at a given distance of the surface, and then a solvent cavity wall that becomes more distant from the surface, thus decreasing the capacitance (*vide supra*). A possible improvement for the electric properties of the interface would be either to use a constant cutoff radius for the cavities or explicit solvent at the interface, which should strongly reduce these problems. Nevertheless, for many systems, the studied potential range is limited, the impact of the capacitance change on the energetic should then remain limited, but this can be problematic while studying large ranges of potential: in this case, a more realistic structure of the electrolyte/electrode interface would be obtained by adding explicit solvent molecules.

IV. RESULTS AND DISCUSSION

(A). Effect of Implicit Solvent on Surface Capacitance. In the classic Stern approach,[46] the total surface capacitance can be divided into three components. The first one corresponds to the intrinsic surface capacitance (C_i) arising from self-interaction of added charge on the surface, as shown in a previous paper;[47] the second arises from the solvent polarization at the interface (C_S), and finally a contribution corresponding to the diffuse countercharge distribution (C_d), which allows one to reach electric neutrality. All these capacitances are in series, leading to a total capacitance of $C_T^{-1} = C_i^{-1} + C_S^{-1} + C_d^{-1}$ dominated by the lowest of the three components. In the case of the implicit solvent, C_i is dependent on the surface electronic structure; the diffuse capacitance can be modeled as a classical planar capacitor with a dielectric medium $C_d \approx \epsilon_0 \epsilon_r / d_{vac}$ and the solvent interface $C_S \approx \epsilon_0 \epsilon_r' / r_c$, where ϵ_r' is the effective dielectric constant at the interface. The capacitance extracted from the local potential change with charge allows one to estimate $\epsilon_r' = 29$ with ϵ_r' remaining weakly dependent on the ϵ_r used. This arises from the non-nil electronic density in this region interacting with the spilling of

D

the dielectric media caused by the shape of the cavity function. For large ϵ_r, the total capacitance is dominated by C_i and C_S and becomes only weakly dependent on the interslab size, leading to an electrochemical model that is independent of this parameter.

In this limit, the capacitance of an explicit metal/solvent interface can be decomposed into more-subtle effects as

$$C_T = \frac{e^2}{S(2\eta - P)}$$

where η is the chemical hardness of the surface, which is defined as $\eta = \frac{1}{2}(\partial^2 E/\partial N^2)$; E is the surface energy; N is the number of electrons added to the surface, relative to the uncharged surface; and P is linked to the structural polarization with charging, as discussed in a previous paper.[47] η is mostly associated with the self-interaction (and with the electronic polarization) of the added charge. The second term P is associated with the structural polarization of the structure, in response to the surface charging, and includes the dipolar reorientation involved in the dielectric response. This latter effect allows one to increase, sometimes strongly, the surface capacitance. The way that the implicit solvent parameters control the total surface capacitance then is not exactly similar to what happens at an explicit solvent interface. The implicit solvent should account for the solvent electronic and structural polarization involved in the dipolar molecular response. However, first, because of the high electric field at the interface, a purely linear response of the implicit solvent is a strong approximation and would need to include higher-order nonlinear effects. Second, explicit solvent impacts on the charge repartition, since charge can flow in the first explicit solvent layers, thus reducing the electronic self-interaction and increasing the surface capacitance.[47] The implicit solvent has exactly the opposite effect, preventing charge density in its domain: its stabilizing effect is mainly electrostatic by reducing the spatial zone of high electric field close to the surface. Therefore, the use of a simple implicit solvent can introduce some nonphysical behavior (in particular, the differential capacitance change with potential), in comparison with an explicit one, and should be carefully parametrized. The use of more advanced environment-dependent nonlinear implicit solvent or including a few monolayers of explicit solvent at the interface while using the PCM further away would allow one to obtain a far more realistic representation of the charge structure. Nevertheless, when the active redox species is not at the interface, the simple implicit-solvent/metal interface can be used if the electrochemical parameters (surface charge and surface capacitance) are in the correct range. This can be exemplified by the simple Li electrode redox ($Li^+ + e^- \rightarrow Li_{(bulk)}$), which serves as a reference electrode at an experimental potential of −3.04 V vs ESH.[48]

(B). Testing the Model: Explicit vs Implicit Model. In this case, the sensibility of the calculation parameters at the interface is low and only the proper electrical parameters (i.e., capacitance) close to the equilibrium potential need to be well-reproduced. The redox pair are, in the present case, the Li^+/Li_{bulk}. Equilibrium potential can found by computing a bare Li surface and a bare Li surface in equilibrium with a solvated Li^+. The free electrochemical energies for these two systems were computed and are presented in Figure 6. The Li^+ cation, being the redox active species, must be described correctly. Using a purely implicit EC solvent model, with a Li^+ cation 19 Å away
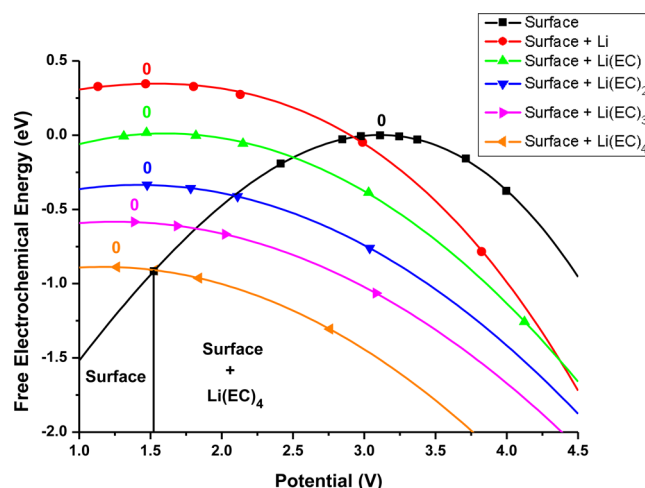

Figure 6. Free electrochemical energy curves for a bare Li surface and a Li surface with a Li^+ attached to different explicit solvent molecules. The potential is referenced to vacuum conditions.

from the surface leads to an equilibrium potential at 2.9 V/vacuum (approximately −1.7 V/NHE). This result is still 1.3 V higher than the experimental values (−3.04 V/NHE), even if it is far more reasonable than the vacuum calculations, leading to a potential of more than 2.0 V/NHE (Li^+ oxidizes water!). The Li^+ cation is only stabilized through electrostatic interactions with the implicit solvent. Therefore, we then have introduced explicit EC molecules, to explicitly account for their strong bonding to Li^+.

(C). Modeling Explicitly Solvated Li^+. The structures of EC[49−51] and solvated Li by EC molecules were previously studied by molecular calculations for different $Li(EC)_n$ ($n = 0−5$) complexes in the molecular limit.[52−55] In these previous studies, only the first four ECs directly coordinate the Li^+; extra ECs only weakly bond with the first coordination sphere formed by the first four strongly bonded ECs, only weakly modifying the energetics. We have built explicit $Li(EC)_n$ ($n = 0−4$) in an implicit solvent at a Li(110) surface for neutral and charged systems (see Figure 6). This allows one to investigate the electric interplay between the surface and the $Li(EC)_n$ complex, including the impact of local electric field and charge transfer, and check the validity of the computed potential scale with the experimental one.

Evaluation of the surface and $Li(EC)_n$ charges can be directly extracted from z-integration of the charge density as these two subparts are separated by a large space without electronic density allowing an unambiguous attribution. In the neutral system, a charge transfer occurs from the $Li(EC)_n$ ($n = 0.4$) to the surface, leading to a strong charge separation: $Li(EC)_n$ structures have a charge of +0.95, while the Li surface has a charge of −0.95. $Li(EC)_n$ structures are then cationic with the proper charge transfer toward the surface. The geometry of all structures remains similar to that which was previously published,[49,52,53] and the changes remain moderate with the system charging. For all potential, $Li(EC)_4$ is the most stable and is stabilized by 1.2 eV, compared to Li^+ in the implicit solvent. Therefore, the first solvation shell of the Li^+ ion is not dependent on the local potential and remains always equal to four EC.

This induces a strong stabilization of the associated free energies, decreasing the equilibrium potential with the Li surface from −1.7 V/NHE for Li^+ to −3.1 V/NHE for

$Li(EC)_4^+$, in quite good agreement with the experimental value. Below -3.1 V, the Li_{bulk} is stable whereas, at higher potential, it is oxidized to $Li(EC)_4^+$. The Li surface only becomes stable when each surface Li is charged by less than -0.062 e/Li; an uncharged Li surface in EC spontaneously transforms into $Li(EC)_4^+ + e^-$.

The associated electrochemical reaction at the equilibrium potential is

$$Li(EC)_4^{0.95+} + Li_{surface}^{0.85-} + 1.1e^- \leftrightarrows Li_{surface}^- + Li_{bulk} + 4EC$$
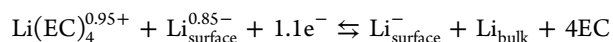
The number of electrons exchanged is 1.1 slightly larger than the expected $1 e^-$. This is the consequence of the $Li(EC)_4^+$ small but non-zero dipole, which shifts the zero-charge potential to 1.26 V (vs vacuum), whereas, for the zero-dipole Li^+ the potential is 1.5 eV. Therefore, there is not only the reduction of the $Li(EC)_4^+$ cation involved, but also a slight reduction of the surface to compensate for the zero-charge potential.

(D). Investigation of the $Li(EC)_4^+$ Reduction. To investigate further the reduction of $Li(EC)_4^+$, the Fukui function of the surface was computed. As previously shown,[16,47] the Fukui function gives mostly the localization of the added electronic charge on the system. In the present case, as shown in Figure 7, added electrons localize homogeneously on the
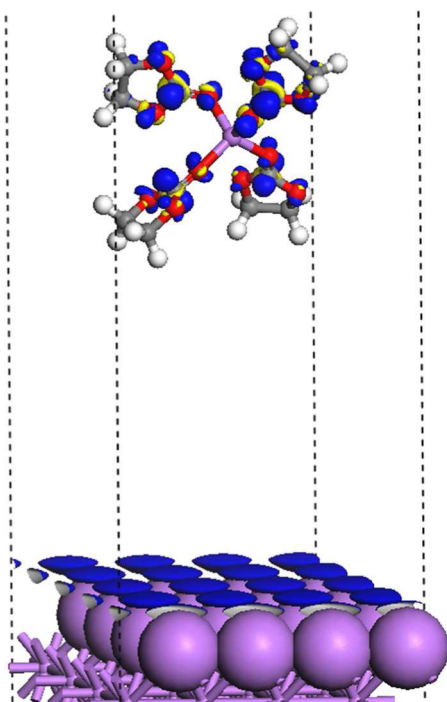

Figure 7. Fukui function of a $Li(EC)_4^+Li(110)$ surface. Blue represents the positive part of the Fukui function, while yellow represents the negative part, corresponding to charge-induced electronic polarization.

surface and in the antibonding π^* orbitals of the carbonates, suggesting that, at this potential, $Li(EC)_4^+$ starts to be reduced mostly by involving the first coordinated EC orbital and not directly the Li. Therefore, this model is important not only to reproduce the proper stability of the cation but also to understand the redox process.

The involvement of the antibonding π^* at the equilibrium potential can be a first hint of the instability of $Li(EC)_4^+$,[56] leading to the formation of a solid electrolyte interface (SEI) that is known to result partly from decomposition of the

solvent. An isolated EC molecule has a highest occupied molecular orbital (HOMO) just above vacuum level, suggesting that it should be very resistant to oxidation. However, the added Li^+ produces an electrophilic activation of the attached ECs, inducing a lowering of the $Li(EC)_4^+$ lowest unoccupied molecular orbital (LUMO) at approximately -4 eV vs vacuum,[57] increasing the sensitivity upon reductive conditions, allowing the filling of the π^* system, weakening the molecular backbone and initiating the formation of the SEI.

V. CONCLUSION

In the present paper, we have investigated the use of a PCM implicit solvent for modeling surface electrochemical properties. First, the use the PCM helps to recover all of the qualitative electric properties, such as capacitance (increasing it by six times, compared to vacuum approaches), and interslab space independence. Therefore, it allows huge progress, compared to previous vacuum calculations. Nevertheless, if the cavity size parameter n_c gives very similar results for wide range of values for nonelectrochemical systems, it becomes critical for electrochemistry, because it strongly modifies the surface capacitance and changes the associated chemistry. This parameter must be carefully checked to get a coherent capacitance in the studied potential region. Another difficulty arises from the differential capacitance given by the implicit solvent that is not fully physical. A way to improve this last point would be either to use explicit solvent close to the surface to include the relevant physical process, or to include a more advanced implicit solvent model, including nonlinear response to the local electric field, as implemented in other codes, and tuning the associated parameters.

An implicit solvent model coupled with an explicit representation of the first solvation shell gives access to surface redox equilibrium processes such as the Li^+/Li redox pair potential or the amount of exchanged electron in the associated process. Furthermore, it also helps to investigate the reduction process of Li^+, showing, in the present case, the involvement of the antibonding π^* system of the carbonates: this can partially give insights in the solvent dissociation mechanism and SEI formation observed experimentally. Finally, these methods could be extended to include the time dimension of solvent–solute complexes[58] by computing *ab initio* molecular dynamics (AIMD) within this mixed implicit/explicit approach at lower computational cost. The ultimate goal is to retain the complexity observed in AIMD calculations of realistic battery materials[59] and to include the electrochemical dimension, while keeping the computational cost low. This could be achieved by using an implicit approach for most of the solvent and restricting the AIMD calculation to the first solvation shell. However, before reaching this goal, the effects of the solvent composition, strong electric fields, and the chemical interaction of the solvent with a surface on the local dielectric properties is still under investigation to improve the PCM approaches used in the case of electrochemical interfaces.

■ AUTHOR INFORMATION

Corresponding Author

*Tel.: 33-4-67-14-46-19. Fax: 33-4-67-14-48-39. E-mail: filhol@univ-montp2.fr.

Notes

The authors declare no competing financial interest.

■ REFERENCES

(1) Dalverny, A. L.; Filhol, J. S.; Doublet, M. L. Interface Electrochemistry in Conversion Materials for Li-Ion Batteries. *J. Mater. Chem.* **2011**, *21*, 10134−10142.

(2) Filhol, J. S.; Combelles, C.; Yazami, R.; Doublet, M. L. Phase Diagrams for Systems with Low Free Energy Variation: A Coupled Theory/Experiments Method Applied to Li-Graphite. *J. Phys. Chem. C* **2008**, *112*, 3982−3988.

(3) Schmickler, W.; Santos, E. *Interfacial Electrochemistry*; Oxford University Press: New York, 1996.

(4) Ben Yahia, M.; Lemoigno, F.; Beuvier, T.; Filhol, J. S.; Richard-Plouet, M.; Brohan, L.; Doublet, M. L. Updated References for the Structural, Electronic, and Vibrational Properties of $TiO_2(B)$ Bulk Using First-Principles Density Functional Theory Calculations. *J. Chem. Phys.* **2009**, *130*, 204501-1−204501-11.

(5) Filhol, J. S.; Saint-Lager, M. C.; De Santis, M.; Dolle, P.; Simon, D.; Baudoing-Savois, R.; Bertolini, J. C.; Sautet, P. Highly Strained Structure of a Four-Layer Deposit of Pd on Ni(110): A Coupled Theoretical and Experimental Study. *Phys. Rev. Lett.* **2002**, *89*, 146106-1−146106-4.

(6) Filhol, J. S.; Simon, D.; Sautet, P. Understanding the High Activity of a Nanostructured Catalyst Obtained by a Deposit of Pd on Ni: First Principle Calculations. *J. Am. Chem. Soc.* **2004**, *126*, 3228−3233.

(7) Filhol, J. S.; Neurock, M. Elucidation of the Electrochemical Activation of Water over Pd by First Principles. *Angew. Chem., Int. Ed.* **2006**, *45*, 402−406.

(8) Mamatkulov, M.; Filhol, J. S. An Ab Initio Study of Electrochemical Vs. Electromechanical Properties: The Case of Co Adsorbed on a Pt(111) Surface. *Phys. Chem. Chem. Phys.* **2011**, *13*, 7675−7684.

(9) Taylor, C. D.; Wasileski, S. A.; Filhol, J. S.; Neurock, M. First Principles Reaction Modeling of the Electrochemical Interface: Consideration and Calculation of a Tunable Surface Potential from Atomic and Electronic Structure. *Phys. Rev. B* **2006**, *73*, 165402-1−165402-16.

(10) Anderson, A. B.; Albu, T. V. *Ab Initio* Determination of Reversible Potentials and Activation Energies for Outer-Sphere Oxygen Reduction to Water and the Reverse Oxidation Reaction. *J. Am. Chem. Soc.* **1999**, *121*, 11855−11863.

(11) Lozovoi, A. Y.; Alavi, A. Reconstruction of Charged Surfaces: General Trends and a Case Study of Pt(110) and Au(110). *Phys. Rev. B* **2003**, *68*, 245416-1−245416-18.

(12) Norskov, J. K.; Rossmeisl, J.; Logadottir, A.; Lindqvist, L.; Kitchin, J. R.; Bligaard, T.; Jonsson, H. Origin of the Overpotential for Oxygen Reduction at a Fuel-Cell Cathode. *J. Phys. Chem. B* **2004**, *108*, 17886−17892.

(13) Otani, M.; Sugino, O. First-Principles Calculations of Charged Surfaces and Interfaces: A Plane-Wave Nonrepeated Slab Approach. *Phys. Rev. B* **2006**, *73*, 115407-1−115407-11.

(14) Bonnet, N.; Dabo, I.; Marzari, N. Chemisorbed Molecules under Potential Bias: Detailed Insights from First-Principles Vibrational Spectroscopies. *Electrochim. Acta* **2014**, *121*, 210−214.

(15) Filhol, J. S.; Bocquet, M. L. Charge Control of the Water Monolayer/Pd Interface. *Chem. Phys. Lett.* **2007**, *438*, 203−207.

(16) Filhol, J. S.; Doublet, M. L. An Ab Initio Study of Surface Electrochemical Disproportionation: The Case of a Water Monolayer Adsorbed on a Pd(111) Surface. *Catal. Today* **2013**, *202*, 87−97.

(17) Lespes, N.; Filhol, J. S. Using the Electrochemical Dimension to Build Water/Ru(0001) Phase Diagram. *Surf. Sci.* **2015**, *631*, 8−16.

(18) Ando, K.; Hynes, J. T. Molecular Mechanism of HCl Acid Ionization in Water: *Ab Initio* Potential Energy Surfaces and Monte Carlo Simulations. *J. Phys. Chem. B* **1997**, *101*, 10464−10478.

(19) Del Popolo, M. G.; Lynden-Bell, R. M.; Kohanoff, J. *Ab Initio* Molecular Dynamics Simulation of a Room Temperature Ionic Liquid. *J. Phys. Chem. B* **2005**, *109*, 5895−5902.

(20) Tomasi, J.; Mennucci, B.; Cammi, R. Quantum Mechanical Continuum Solvation Models. *Chem. Rev.* **2005**, *105*, 2999−3093.

(21) Cossi, M.; Rega, N.; Scalmani, G.; Barone, V. Energies, Structures, and Electronic Properties of Molecules in Solution with the C-PCM Solvation Model. *J. Comput. Chem.* **2003**, *24*, 669−681.

(22) Jinnouchi, R.; Anderson, A. B. Electronic Structure Calculations of Liquid−Solid Interfaces: Combination of Density Functional Theory and Modified Poisson−Boltzmann Theory. *Phys. Rev. B* **2008**, *77*, 245417-1−245417-18.

(23) Andreussi, O.; Dabo, I.; Marzari, N. Revised Self-Consistent Continuum Solvation in Electronic-Structure Calculations. *J. Chem. Phys.* **2012**, *136*, 064102-1−064102-20.

(24) Letchworth-Weaver, K.; Arias, T. A. Joint Density Functional Theory of the Electrode-Electrolyte Interface: Application to Fixed Electrode Potentials, Interfacial Capacitances, and Potentials of Zero Charge. *Phys. Rev. B* **2012**, *86*, 075140-1−075140-16.

(25) Mathew, K.; Sundararaman, R.; Letchworth-Weaver, K.; Arias, T. A.; Hennig, R. G. Implicit Solvation Model for Density-Functional Study of Nanocrystal Surfaces and Reaction Pathways. *J. Chem. Phys.* **2014**, *140*, 084106-1−084106-8.

(26) Brissot, C.; Rosso, M.; Chazalviel, J. N.; Lascaud, S. Dendritic Growth Mechanisms in Lithium/Polymer Cells. *J. Power Sources* **1999**, *81*, 925−929.

(27) Rosso, M.; Brissot, C.; Teyssot, A.; Dolle, M.; Sannier, L.; Tarascon, J. M.; Bouchetc, R.; Lascaud, S. Dendrite Short-Circuit and Fuse Effect on Li/Polymer/Li Cells. *Electrochim. Acta* **2006**, *51*, 5334−5340.

(28) Akolkar, R. Mathematical Model of the Dendritic Growth During Lithium Electrodeposition. *J. Power Sources* **2013**, *232*, 23−28.

(29) Park, M. S.; Ma, S. B.; Lee, D. J.; Im, D.; Doo, S. G.; Yamamoto, O. A Highly Reversible Lithium Metal Anode. *Sci. Rep.* **2014**, *4*, 3815-1−3815-8.

(30) Bridel, J. S.; Grugeon, S.; Laruelle, S.; Hassoun, J.; Reale, P.; Scrosati, B.; Tarascon, J. M. Decomposition of Ethylene Carbonate on Electrodeposited Metal Thin Film Anode. *J. Power Sources* **2010**, *195*, 2036−2043.

(31) Leung, K. Electronic Structure Modeling of Electrochemical Reactions at Electrode/Electrolyte Interfaces in Lithium Ion Batteries. *J. Phys. Chem. C* **2013**, *117*, 1539−1547.

(32) Leung, K. Two-Electron Reduction of Ethylene Carbonate: A Quantum Chemistry Re-Examination of Mechanisms. *Chem. Phys. Lett.* **2013**, *568*, 1−8.

(33) Li, T.; Balbuena, P. B. Theoretical Studies of the Reduction of Ethylene Carbonate. *Chem. Phys. Lett.* **2000**, *317*, 421−429.

(34) Leung, K.; Qi, Y.; Zavadil, K. R.; Jung, Y. S.; Dillon, A. C.; Cavanagh, A. S.; Lee, S. H.; George, S. M. Using Atomic Layer Deposition to Hinder Solvent Decomposition in Lithium Ion Batteries: First-Principles Modeling and Experimental Studies. *J. Am. Chem. Soc.* **2011**, *133*, 14741−14754.

(35) Perdew, J. P.; Burke, K.; Ernzerhof, M. Generalized Gradient Approximation Made Simple. *Phys. Rev. Lett.* **1996**, *77*, 3865−3868.

(36) Blochl, P. E. Projector Augmented-Wave Method. *Phys. Rev. B* **1994**, *50*, 17953−17979.

(37) Kresse, G.; Joubert, D. From Ultrasoft Pseudopotentials to the Projector Augmented-Wave Method. *Phys. Rev. B* **1999**, *59*, 1758−1775.

(38) Kresse, G.; Furthmuller, J. Efficiency of *Ab-Initio* Total Energy Calculations for Metals and Semiconductors Using a Plane-Wave Basis Set. *Comput. Mater. Sci.* **1996**, *6*, 15−50.

(39) Kresse, G.; Hafner, J. *Ab-Initio* Molecular-Dynamics Simulation of the Liquid−Metal Amorphous−Semiconductor Transition in Germanium. *Phys. Rev. B* **1994**, *49*, 14251−14269.

(40) Rousseau, R.; Marx, D. Exploring the Electronic Structure of Elemental Lithium: From Small Molecules to Nanoclusters, Bulk Metal, and Surfaces. *Chem.—Eur. J.* **2000**, *6*, 2982−2993.

(41) Doll, K.; Harrison, N. M.; Saunders, V. R. A Density Functional Study of Lithium Bulk and Surfaces. *J. Phys.: Condens. Matter* **1999**, *11*, 5007−5019.

(42) Reiss, H. The Fermi Level and the Redox Potential. *J. Phys. Chem.* **1985**, *89*, 3783−3791.

(43) Rossmeisl, J.; Norskov, J. K.; Taylor, C. D.; Janik, M. J.; Neurock, M. Calculated Phase Diagrams for the Electrochemical Oxidation and Reduction of Water over Pt(111). *J. Phys. Chem. B* **2006**, *110*, 21833−21839.

(44) Fishman, M.; Zhuang, H. L.; Mathew, K.; Dirschka, W.; Hennig, R. G. Accuracy of Exchange-Correlation Functionals and Effect of Solvation on the Surface Energy of Copper. *Phys. Rev. B* **2013**, *87*, 245402-1−245402-7.

(45) Hatlo, M. M.; van Roij, R.; Lue, L. The Electric Double Layer at High Surface Potentials: The Influence of Excess Ion Polarizability. *Europhys. Lett.* **2012**, *97*, 28010-1−28010-6.

(46) Macdonald, J. R.; Barlow, C. A. Theory of Double-Layer Differential Capacitance in Electrolytes. *J. Chem. Phys.* **1962**, *36*, 3062−3080.

(47) Filhol, J. S.; Doublet, M. L. Conceptual Surface Electrochemistry and New Redox Descriptors. *J. Phys. Chem. C* **2014**, *118*, 19023−19031.

(48) Trasatti, S. The Absolute Electrode Potential—An Explanatory Note (Recommendations 1986). *Pure Appl. Chem.* **1986**, *58*, 955−966.

(49) Alonso, J. L.; Cervellati, R.; Degli Esposti, A.; Lister, D. G.; Palmieri, P. Microwave-Spectrum and Abinitio Computations for Ethylene Carbonate. 1. Conformation and Ring Inversion. *J. Chem. Soc., Faraday Trans.* **1986**, *82*, 337−356.

(50) Masia, M.; Probst, M.; Rey, R. Ethylene Carbonate-Li$^+$: A Theoretical Study of Structural and Vibrational Properties in Gas and Liquid Phases. *J. Phys. Chem. B* **2004**, *108*, 2016−2027.

(51) Silva, L. B.; Freitas, L. C. G. Structural and Thermodynamic Properties of Liquid Ethylene Carbonate and Propylene Carbonate by Monte Carlo Simulations. *J. Mol. Struct., THEOCHEM* **2007**, *806*, 23−34.

(52) Bhatt, M. D.; Cho, M.; Cho, K. Interaction of Li$^+$ Ions with Ethylene Carbonate (EC): Density Functional Theory Calculations. *Appl. Surf. Sci.* **2010**, *257*, 1463−1468.

(53) Bhatt, M. D.; Cho, M.; Cho, K. Conduction of Li$^+$ Cations in Ethylene Carbonate (EC) and Propylene Carbonate (PC): Comparative Studies Using Density Functional Theory. *J. Solid State Electrochem.* **2012**, *16*, 435−441.

(54) Tachikawa, H.; Abe, S. Solvent Stripping Dynamics of Lithium Ion Solvated by Ethylene Carbonates: A Direct *Ab-Initio* Molecular (AIMD) Study. *Electrochim. Acta* **2014**, *120*, 57−64.

(55) Skarmoutsos, I.; Ponnuchamy, V.; Vetere, V.; Mossa, S. Li$^+$ Solvation in Pure, Binary and Ternary Mixtures of Organic Carbonate Electrolytes. *J. Phys. Chem. C* **2015**, *119*, 4502−4515.

(56) Aurbach, D.; Zaban, A.; Schechter, A.; Eineli, Y.; Zinigrad, E.; Markovsky, B. The Study of Electrolyte-Solutions Based on Ethylene and Diethyl Carbonates for Rechargeable Li Batteries. 1. Li Metal Anodes. *J. Electrochem. Soc.* **1995**, *142*, 2873−2882.

(57) Ponnuchamy, V. *Toward a Better Understanding of Lithium Ion Local Environment in Pure, Binary and Ternary Mixtures of Carbonates Solvents: A Numerical Approach*. Université de Grenoble, Grenoble, France, 2015.

(58) Ganesh, P.; Jiang, D. E.; Kent, P. R. C. Accurate Static and Dynamic Properties of Liquid Electrolytes for Li-Ion Batteries from *Ab Initio* Molecular Dynamics. *J. Phys. Chem. B* **2011**, *115*, 3085−3090.

(59) Ganesh, P.; Kent, P. R. C.; Jiang, D. E. Solid-Electrolyte Interphase Formation and Electrolyte Reduction at Li-Ion Battery Graphite Anodes: Insights from First-Principles Molecular Dynamics. *J. Phys. Chem. C* **2012**, *116*, 24476−24481.